IJNAOE
©SNAK, 2015

Int. J. Nav. Archit. Ocean Eng. (2015) 7:739~749
http://dx.doi.org/10.1515/ijnaoe-2015-0052
pISSN: 2092-6782, eISSN: 2092-6790

Design of the dual-buoy wave energy converter based on actual wave data of East Sea

Jeongrok Kim[1], Hyuck-Min Kweon[2], Weon-Mu Jeong[3], Il-Hyoung Cho[4] and Hong-Yeon Cho[5]

[1]*Department of Ocean System Engineering, Jeju National University, Jeju, Korea*
[2]*Department of Railway Construction and Environmental Engineering, Gyeongju University, Gyeongbuk, Korea*
[3]*Marine Environments & Conservation Research Department, Korea Institute of Ocean Science & Technology, Gyeonggi, Korea*
[4]*Department of Ocean System Engineering, Jeju National University, Jeju, Korea*
[5]*Marine Environments & Conservation Research Department, Korea Institute of Ocean Science & Technology, Gyeonggi, Korea*

Received 3 January 2015; Revised 17 May 2015; Accepted 31 May 2015

ABSTRACT: *A new conceptual dual-buoy Wave Energy Converter (WEC) for the enhancement of energy extraction efficiency is suggested. Based on actual wave data, the design process for the suggested WEC is conducted in such a way as to ensure that it is suitable in real sea. Actual wave data measured in Korea's East Sea (position: 36.404 N° and 129.274 E°) from May 1, 2002 to March 29, 2005 were used as the input wave spectrum for the performance estimation of the dual-buoy WEC. The suggested WEC, a point absorber type, consists of two concentric floating circular cylinders (an inner and a hollow outer buoy). Multiple resonant frequencies in proposed WEC affect the Power Ttake-off (PTO) performance of the WEC. Based on the numerical results, several design strategies are proposed to further enhance the extraction efficiency, including intentional mismatching among the heave natural frequencies of dual buoys, the natural frequency of the internal fluid, and the peak frequency of the input wave spectrum.*

KEY WORDS: Dual-buoy wave energy converter; Multiple resonance; Measured wave data; Relative heave motion; Extracted power; Linear electric generator.

INTRODUCTION

With the increasing demand for renewable energy sources, many countries are responding positively by taking constructive measures such as the reduction of carbon emissions in an effort to improve the global environment. Renewable energy is sustainable, clean, and unlimited, and comes in diverse forms, such as solar thermal energy, solar photovoltaics, geothermal energy, wind energy, and wave energy. The most suitable method for obtaining renewable energy can be chosen according to the regional and environmental characteristics. While some forms of renewable energy have been successfully commercialized, most are still being researched and developed.

Corresponding author: *Hyuck-Min Kweon*, e-mail: *choiziwon@daum.net*

Of the various sources of renewable energy, wave energy has the highest energy density. Wave Energy Converters (WEC), which extract electrical energy from wave energy, are known to be the least hazardous to surrounding environments (Drew et al., 2009). In addition, WEC technology has been researched extensively in Europe and Japan for use with the abundant wave energy available in those regions. Thus, some WECs have been successfully commercialized (Power Buoy, LIMPET), and many WECs are still being researched for commercialization (Mekhiche et al., 2014; Boake et al., 2002).

The WECs developed thus far are classified into attenuators, point absorbers and terminators, according to their method of power generation (Drew et al., 2009; Soares et al., 2014). Of these, the point absorber type, which extracts wave energy from the heaving motion of a WEC device, is not affected by the direction of the incident waves and its motion is highly amplified when its natural frequency agrees with the wave frequency. Since the beginning of wave energy research, research into increasing energy absorption has been focused on tuning the system to oscillate in resonance with the incoming wave. It is well known that a point absorber system in resonance with the incident wave will achieve increased amplitude and speed, and therefore, transfers more energy than a system working off resonance (Budar and Falnes, 1975; Falnes, 2002).

However, the frequency bandwidth capable of producing the highly amplified motion responses by resonance is limited. Therefore, although the energy extraction efficiency may increase by resonance, the narrow resonant frequency bandwidth restricts the ability to obtain a larger amount of energy from irregular waves that contain many different frequencies. To overcome such limitations, this study proposes a dual-buoy WEC that can generate multiple resonances. Multiple resonances constitute the most significant feature of the proposed dual-buoy WEC and enable the resonance of the wave converter system at different frequencies, thereby allowing for the extraction of energy from a wider frequency bandwidth.

The PowerBuoy, Wavebob (Weber et al., 2009) and AquaBuOY (Weinstein et al., 2004), which are currently utilized, are typical floating two-body WECs of the point absorber variety. The PowerBuoy does not use the resonance concept. It consists of an inner buoy with a relatively long draft, and a hollow outer buoy with a shorter draft. In this model, the inner buoy's heave motion is considerably reduced by the damping plate attached to the bottom of the inner buoy, and the outer buoy tends to follow the waves. The relative heave motion between the two is used to extract electrical energy. Wavebob, with a shape similar to the power buoy, can extract a larger amount of power using the resonance of the inner buoy, compared to the PowerBuoy. To solve the radiation problem of concentric dual-buoy WECs, Mavrakos (2005) used the matched eigenfunction expansion method to compute the hydrodynamic properties of each buoy, taking into account the interference effects. Bae and Cho (2013) investigated the diffraction and radiation problems of hollow circular cylinders and addressed the characteristics of heaving motion using the eigenfunction expansion method. Sinha et al. (2014) investigated the optimal array method and the wave interaction due to multiple point absorber WECs for maximizing wave energy extraction as possible as they can.

Numerical results obtained from investigating the effect of a dual-buoy's hydrodynamic interactions on the performance characteristics of a WEC are presented here. The numerical model based on the ANSYS AQWA commercial code included all interactions among the participating dual buoys arranged concentrically. The relative heave responses of a dual-buoy WEC, using the input wave spectrum measured at two sites in Hupo Harbor, were examined for the on/off status of the device. A considerable increase in the absorbed power was observed if multiple resonant frequencies were distributed around the peak frequency of the wave spectrum. We intentionally applied a mismatch between the heave resonant frequency of the outer buoy and the resonant frequency of the internal fluid by attaching a concentric external torus. Future work is currently under way to investigate in more detail the various damping mechanisms associated with the mechanical friction between the two buoys as well as with the LEG and the PTO system.

MULTIPLE RESONANCE OF A DUAL-BUOY WEC

The conventional WEC system consists of a cylindrical inner buoy and a hollow outer buoy, with a gap between the two. The PTO system used for the generation of electrical energy employs a LEG, consisting of a permanent magnet fixed to the outer buoy and a coil attached to the top of the inner buoy. Electrical energy is produced from the relative heave motion of each buoy. Thus, it is very important to increase the relative heave motion of the two buoys. To that end, the multiple resonance concept is adopted herein.

The proposed WEC system has three natural frequencies: the two heave natural frequencies, one for the inner buoy and another for the outer buoy, and the piston-mode natural frequency of the internal fluid that exists between the inner and the

outer buoys (see Fig. 1). If the incident wave frequency corresponds to the natural frequency, the heave motion of the two buoys and the internal fluid can increase rapidly due to resonance. In fact, the inner buoy's motion does not increase much at the inner buoy's resonant frequency. The inner buoy, which is situated within the internal fluid region, moves in accordance with the internal fluid column, and its motion is largely amplified at the internal fluid's resonant frequency.

The heave natural frequency ($\omega_{Ni}, i = 1, 2$) of the inner and outer buoys was calculated as shown in Eq. (1). Correspondingly, the natural frequency (ω_{Nf}) of the internal fluid is shown in Eq. (2) as originally proposed by Fukuda (1977), wherein $i = 1$ represents the inner buoy, $i = 2$ represents the outer buoy, m_i denotes the buoy's mass, a_{ii} the added mass, ρ the water density, g the gravity acceleration, A_{Wi} the buoy's water plane area, and A_f the internal fluid's cross-sectional area. In Fig. 1, the additional torus-shaped structure is attached to the outer buoy. It increases the water plane area of the outer buoy, widening the gap between the natural frequency of the internal fluid and the heave natural frequency of the outer buoy.

$$\omega_{Ni} = \sqrt{\frac{\rho g A_{Wi}}{m_i + a_{ii}}}, \quad (i = 1, 2) \tag{1}$$

$$\omega_{Nf} = \sqrt{\frac{g}{d_2 + 0.41\sqrt{A_f}}} \tag{2}$$

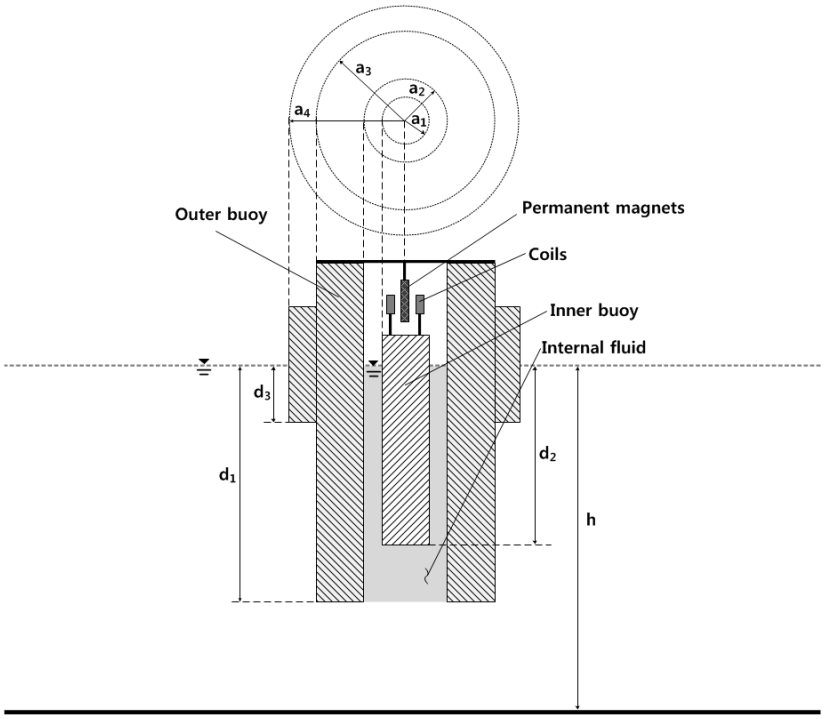

Fig. 1 Definition sketch of the dual-buoy wave energy converter.

WAVE MEASUREMENT IN REAL SEA

Wave data were measured at two sites (W1 and W2) in Hupo Harbor, in the East Sea of Korea, as shown in Fig. 2. The two sites are located in shallow waters, with a water depth of 9.5 *m* at W1 and a water depth of 18.5 *m* at W2. The W1 area is partly shielded from the winter NE storm wave, while W2 is located in fully open waters. For the wave measurement, a pressure-type wave gauge [Wave and Tide Gauge (WTG)] was used. The observation period, installation position, water depth, number of data points, and observation rate, are shown in Table 1. The data gathering time step for the WTG was 0.5 *sec.*, and the wave spectrum was produced by applying the FFT (Fast Fourier Transform) technique using 2,048 data points every 30 minutes.

Fig. 2 Wave measurement sites in Hupo Harbor.

Table 1 Basic information on the two sites.

Station ID	W1	W2
Observation period	2002.05.01-2005.03.31	2008.06.01-2012.05.31
Geographical coordinates	36.404N°, 129.274E°	36.700N°, 129.484E°
Water depth (*m*)	9.5	18.5
No. of data	45,223	68,817
Observation rate (Missing ratio, %)	88.3% (11.7%)	98.1% (1.9%)

WAVE DATA ANALYSIS METHOD AND WAVE ENERGY SPECTRUM

Since the WEC produces electrical energy from the incident waves that form on a typical day, the analysis of the wave data on typical days should be prioritized. Fig. 3 provides useful information for the most frequent wave period and wave height in one year, and shows the joint probability distribution of the significant wave height and mean wave period at sites W1 and W2. At the two sites, the mean wave period ranges from 3.5 *sec.* to 7.5 *sec.*, and the significant wave height is less than 1.5 *m*. In addition, the peak period is 4-5 *sec.* at W1 and 5-5.5 *sec.* at W2. Many of the waves appear frequently in the wide range of wave periods. Meanwhile, the most frequent wave height is about 0.5 *m*. This indicates that the installation site produces extremely low energy density, which is suitable for the operation of the present WEC. This is because the dual-buoy WEC can extract wave energy in a wide frequency bandwidth and improve the energy extraction efficiency using multiple resonances. The proposed dual-buoy WEC was designed based on the W1 wave data.

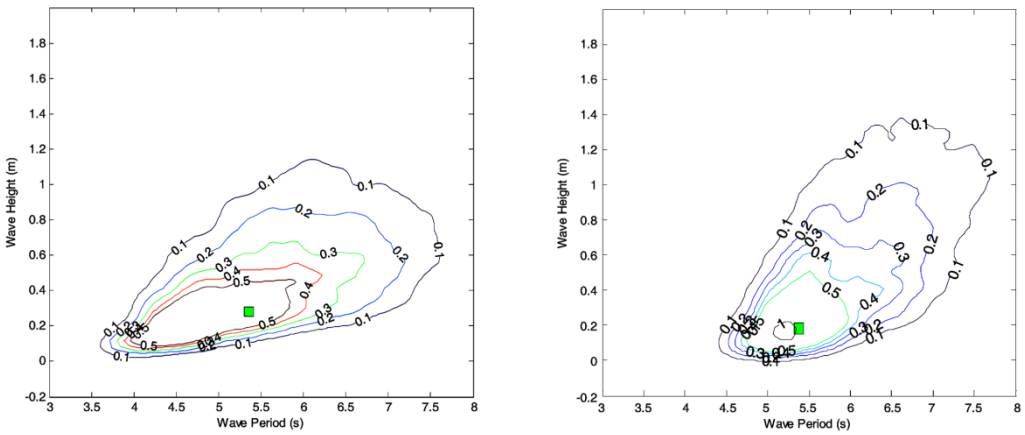

(a) St. W1. (b) St. W2.

Fig. 3 Joint probability distributions of the significant wave height and the mean wave period measured at sites W1 and W2.

In this section, the wave spectrum is introduced based on the data measured at the two sites. Kweon et al. (2013) reported that the wave energy distribution at the installation site cannot be expressed in terms of the existing standard wave spectrum, such as JONSWAP and ITTC, and instead proposed the Generalized Extreme Value (GEV) in the form of a cumulative distribution function.

The GEV is shown in the cumulative distribution function presented in Eq. (3), where μ represents the location parameter, σ represents the scale parameter, and ξ represents the shape parameter. With the cumulative distribution function, the probability density function can be calculated using $p = dP / df$ and is expressed in Eq. (4).

$$P(f;\mu,\sigma,\xi) = \exp\left\{-\left[1+\xi\left(\frac{f-\mu}{\sigma}\right)\right]^{-1/\xi}\right\}, \quad 1+\xi(f-\mu)/\sigma > 0 \tag{3}$$

$$p(f;\mu,\sigma,\xi) = \frac{1}{\sigma}\left[1+\xi\left(\frac{f-\mu}{\sigma}\right)\right]^{(-1/\xi)-1} \exp\left\{-\left[1+\xi\left(\frac{f-\mu}{\sigma}\right)\right]^{-1/\xi}\right\} \tag{4}$$
$$1+\xi(f-\mu)/\sigma > 0$$

As shown in Eq. (5), the conversion coefficient (k) denotes the area under the observed averaged wave spectrum curve, where n represents the total number of frequencies, which is fixed at 60 in the present study. The corresponding frequency interval df was calculated to be 1/128 *Hz*. Therefore, the probability density function by the average wave spectrum at the installation site can be expressed as Eq. (6).

$$k = \sum_{i=1}^{n} S(f_i)_{obs} df \tag{5}$$

$$S(f)_{fit} = k \cdot p(f;\mu,\sigma,\xi), \text{ where } \int p(f;\mu,\sigma,\xi)df = 1 \tag{6}$$

In Eqn. (6), the conversion coefficient k is dependent on the area of the observed wave spectrum. For the wave data at the two sites and the target design data (with significant wave height less than 0.5 *m* and within the average period of 4–6 *sec*), the corresponding parameters in Eqn. (4) were estimated using the maximum likelihood method. These are listed in Table 2 with regard to the total wave spectrum and the selected wave spectrum at W1 and W2.

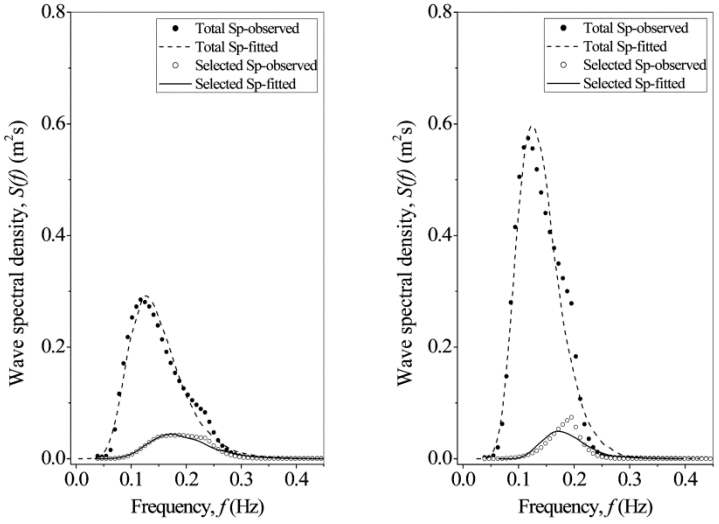

Fig. 4 Wave spectrum from the total and selected wave data at the two sites (W1, W2).

Fig. 4 shows the wave spectrum using Eqn. (4) and the parameters expressed in Table 2. The total wave spectrum (•) obtained from the total wave data differs significantly according to the site. However, comparisons between the selected wave spectrum (◦) belonging to significant wave heights of less than 0.5 *m*, and within the average period of 4–6 *s*, show little or no difference between the two sites. The area under each wave spectrum curve is represented by the conversion coefficient listed in Table 2. In particular, the total wave spectrum at W1 was smaller than that at W2, but the selected wave spectrum based on the selected range of both the wave height and the wave period was slightly greater than that at W2.

Table 2 Design parameters for the total and selected wave spectrum at W1 and W2.

Item		W1	W2
Total wave spectrum	GEV-1 (ξ)	-0.0121	-0.0537
	GEV-2 (σ)	0.041	0.0336
	GEV-3 (μ)	0.1264	0.1223
	Conversion coefficient (k)	0.032556	0.055201
Selected wave spectrum	GEV-1 (ξ)	-0.0801	-0.0761
	GEV-2 (σ)	0.0466	0.0345
	GEV-3 (μ)	0.1693	0.1618
	Conversion coefficient (k)	0.005731575	0.004646663

DESIGN AND SIMULATION OF THE DUAL BUOY

It is possible to design an optimal shape for the dual-buoy WEC with the selected wave spectrums at site W1, as depicted in Table 2. First, the dual-buoy WEC was designed to identify two natural frequencies (one for the outer buoy, and one for the internal fluid) near the peak frequency of the wave spectrum, based on the total wave data. Second, the dual-buoy WEC was designed to match the two natural frequencies with the most frequently observed wave frequency of the wave spectrum, based on the selected wave data. The latter method was adopted herein to extract more energy from a dual-buoy WEC where the target site was W1.

The most frequently observed wave frequency bandwidth, as shown in Fig. 4, was 0.167-0.25 *Hz* (1.05-1.57 *rad/s*). Thus, the dual-buoy WEC was designed so that the outer buoy's heaving natural frequency could be located at 0.24 *Hz* (1.5 *rad/s*), and the internal fluid's natural frequency could be located at 0.197 *Hz* (1.24 *rad/s*). The specifications for the designed dual-buoy WEC are summarized in Table 3. Better results could have been obtained by positioning the natural frequency of the internal fluid at 0.167 *Hz* (1.05 *rad/s*). However, this choice makes the draft for the outer buoy very long, increasing the risk of the buoy hitting the sea bottom and becoming damaged. Therefore, considering the water depth of 10m at the installation site, and the heave displacement, the draft for the outer buoy was determined to be 6 *m*.

Table 3 Specification of a dual-buoy WEC.

Item	Radius (*m*)	Draft (*m*)	Mass (*kg*)	Natural frequency (*rad/sec*)	
Inner buoy	0.35 (a_1)	5.0 (d_2)	1972.3	Inner buoy	1.34
Outer buoy	0.55 (a_2)	6.0 (d_1)	7366.1	Internal fluid	1.24
	0.80 (a_3)	1.0 (d_3)		Outer buoy	1.50
	0.95 (a_4)				

As mentioned earlier, the average period at site W1 was 4-6 *sec.*, and the corresponding significant wave height was 0.5 *m*. The wave height is an additional important factor in the design of an LEG. Considering the shape and heave displacement of the buoy, the maximum LEG stroke was determined to be 1.5 *m* ($= 0.5m \times 3$), whereas the heave RAO (Response Amplitude Operator) was assumed to be 3 at the resonant frequency.

Considering the maximum stroke of LEG, the appropriate wave period and the wave height are limited for power extraction. Thus, from the recorded wave data, only the effective waves from which energy could be extracted were selected to reproduce the wave spectrum. The selected Sp-fitted spectrum was selected as the input wave spectrum for motion analysis (see Fig. 4).

To obtain the dual buoy's heave motion responses ($\zeta = \mathrm{Re}\left\{\xi e^{-i\omega t}\right\}$), the equation for motion should be solved. Eq. (7) shows the heave-motion equation of the two buoys in the frequency domain, where $\left[\xi\right] = \left(\xi_1, \xi_2\right)^T$ and $\left[f^D\right] = \left(f_1^D, f_2^D\right)^T$ are the heave displacement and the wave exciting force of each buoy, respectively. The mass matrix $\left[M\right]$ and the stiffness matrix $\left[K\right]$ are expressed by Eq. (8).

$$\left\{-\left[M\right]\omega^2 - i\omega\left[B\right] + \left[K\right]\right\}\left[\xi\right] = A\left[f^D\right] \tag{7}$$

$$[M] = \begin{bmatrix} m_1 + a_{11}(\omega) & a_{12}(\omega) \\ a_{21}(\omega) & m_2 + a_{22}(\omega) \end{bmatrix}, [K] = \begin{bmatrix} \rho g A_{W1} & 0 \\ 0 & \rho g A_{W2} \end{bmatrix}. \tag{8}$$

where m_1 and m_2 are the masses of the inner and outer buoys, respectively, $A_{W1}(=\pi a_1^2)$ and $A_{W2}(=\pi(a_4^2 - a_2^2))$ are the water plane areas for the inner and outer buoys, and $a_{ij}(\omega)$ is the frequency dependent added mass.

The damping matrix $\left[B\right]$ is expressed as follows:

$$[B] = \begin{bmatrix} b_{11}(\omega) + b_{v1} + c_{PTO} & b_{12}(\omega) - c_{PTO} \\ b_{21}(\omega) - c_{PTO} & b_{22}(\omega) + b_{v2} + c_{PTO} \end{bmatrix}, \tag{9}$$

In Eq. (9), $b_{ij}(\omega)$ is the radiation damping coefficient, and c_{PTO} is the PTO damping coefficient generated when extracting electrical energy through the LEG. In addition, $b_{vi}(i = 1, 2)$ are the viscous damping coefficients, which cannot be obtained using the present potential theory. Thus, the viscous damping coefficients were determined from the free-decay model test (scale ratio=1/5.95). The viscous damping coefficient is represented by Eq. (10), where the non-dimensional viscous damping coefficient, κ_i, can be obtained from the set of successive heave amplitudes. This decay test revealed that $\kappa_1 = 0.082$ and $\kappa_2 = 0.059$.

$$b_{vi} = \frac{2\kappa_i K_{ii}}{\omega_{Ni}}, (i = 1, 2) \tag{10}$$

In the heave-motion equation of a dual-buoy WEC, the added mass, radiation damping coefficients, and wave exciting force were obtained using ANSYS AQWA commercial code, based on the linear potential theory. The time-averaged power is expressed by Eq. (11), where A is the amplitude of the incident wave.

$$\frac{\overline{P}(\omega)}{A^2} = \frac{1}{2} c_{PTO} \omega^2 \left| \frac{\xi_1(\omega) - \xi_2(\omega)}{A} \right|^2, \tag{11}$$

If the wave spectrum ($S(\omega)$) of the installation site is given, the relative heave-motion spectrum ($S_{\xi_{1/2}}(\omega)$), and the power spectrum ($S_{\sqrt{P}}(\omega)$) can be evaluated as in Eq. (12).

$$S_{\xi_{1/2}}(\omega)=\left|\frac{\xi_1(\omega)-\xi_2(\omega)}{A}\right|^2\cdot S(\omega),$$
$$S_{\sqrt{P}}(\omega)=\frac{\overline{P}(\omega)}{A^2}\cdot S(\omega). \tag{12}$$

The significant wave height, significant relative-heave-motion amplitude, and significant amplitude of the square root power in irregular waves can then be obtained from

$$H_{1/3}=4\sqrt{\int_0^\infty S(\omega)d\omega},\ (\xi_{1/2})_{1/3}=2\sqrt{\int_0^\infty S_{\xi_{1/2}}(\omega)d\omega},\ \sqrt{P_{1/3}}=2\sqrt{\int_0^\infty S_{\sqrt{P}}(\omega)d\omega} \tag{13}$$

Figs. 5 to 7 show the numerical results for the dual-buoy WEC with the specifications summarized in Table 3. First, Fig. 5 shows the heave RAO $(|\xi_1|/A, |\xi_2|/A)$ of the inner and outer buoys as well as the relative heave RAO $(|\xi_{1/2}|/A)$ between them without taking into consideration the viscous damping effect. The heave RAO of the inner buoy, which moves according to the internal fluid, is significantly amplified at the internal fluid's resonant frequency (1.24 *rad/s*). However, outside the resonant frequency, the heave motion decreases considerably. This can also be confirmed with the heave RAO curve of the outer buoy. The outer buoy shows a large heave response at its heave resonant frequency (1.5 *rad/s*) and also decreases significantly, similar to the inner buoy, at frequency ranges outside the resonant frequency. The RAO curve of the relative heave motion has two peaks at 1.24 *rad/s* and 1.5 *rad/s*. In addition, comparatively high RAO values are maintained between the two peaks. This confirms that the proposed dual-buoy WEC can use two resonant frequencies and extract energy in a wide frequency bandwidth between them.

Fig. 6 shows the numerical results related to the viscous damping effects obtained from the free-decay test. Compared to Fig. 5, Fig. 6 shows that the peak value decreases significantly at the two resonant frequencies owing to the effect of viscous damping. The reduction of the peak value was greater for the outer buoy compared to the inner buoy. The viscous damping effect, manifested by (among others) the production of turbulent eddies shed from the additional torus structure (installed to change the outer buoy's heave natural frequency), was greatly increased. The relative heave RAO is about 7.5 at the internal fluid's resonant frequency, and about 3.5 at the outer buoy's heave natural frequency. Moreover, the RAO values are higher than 2 and within the range of the two resonant frequencies, which reconfirms that energy can be extracted in a wider frequency range.

Fig. 7 plots the heave RAO as a function of wave frequency when the PTO damping coefficient $c_{PTO}=1210kg/\mathrm{s}$ is applied. The PTO damping coefficient is selected numerically as the optimal value, which makes the significant amplitude of square root power $(\sqrt{P_{1/3}})$ the maximum. It can be observed that by slightly mismatching the two resonant frequencies (outer buoy and internal fluid), the heave RAO shows a double peak similar to the previous figures. Each heave RAO curve is greatly reduced at resonant frequencies by the PTO damping force. Since the output power is also proportional to the PTO damping coefficients, the output power under the mismatched condition with smaller damping coefficients does not necessarily increase despite the large increase in relative motions, as can be seen in Fig. 7.

Figs. 8 and 9 show the relative heave motion spectrum of a dual-buoy WEC evaluated with the wave spectrum at W1 and W2 (the selected Sp-fitted wave spectrum). Comparison of the two graphs revealed that the two peaks corresponded to the internal fluid's resonant frequency and the outer buoy's heave natural frequency. In addition, the peak value of the relative heave motion spectrum was greater at W1 than at W2, but the shape of the heave motion spectrum at each site was similar. As illustrated in Fig. 7, the area of the relative heave motion spectrum is largely reduced with the PTO installation compared to without.

The numerical simulation revealed that the proposed dual-buoy WEC could not only enhance energy extraction efficiency using multiple resonant frequencies but could also absorb wave energy in a wider wave frequency bandwidth. These results demonstrate that the proposed dual-buoy WEC is suitable for sea sites with low wave energy density, such as Korea's East Sea.

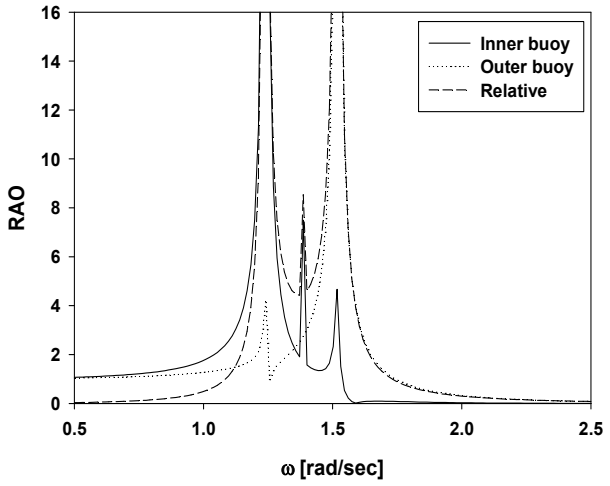

Fig. 5 Heave RAO as a function of the wave frequency for $\kappa_1 = \kappa_2 = 0.0$.

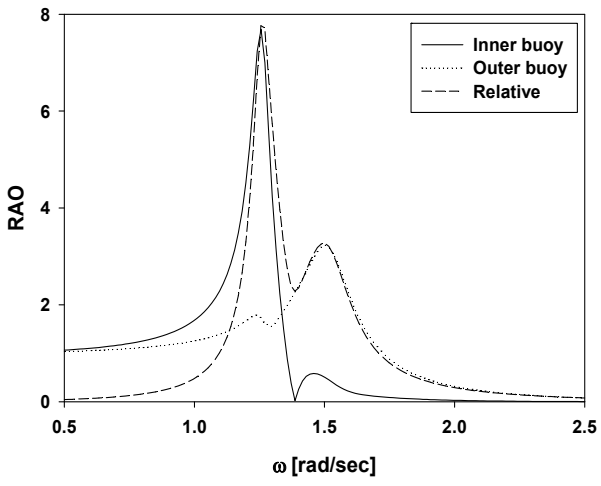

Fig. 6 Heave RAO as a function of the wave frequency for $\kappa_1 = 0.082, \kappa_2 = 0.0592$.

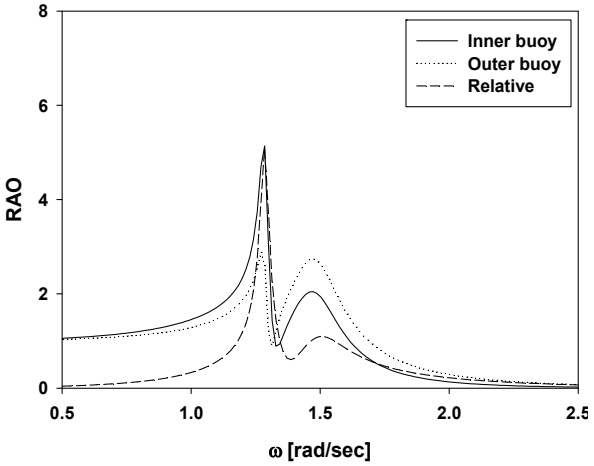

Fig. 7 Heave RAO as a function of the wave frequency for $c_{PTO} = 1210 kg/\sec$ and $\kappa_1 = 0.082, \kappa_2 = 0.0592$.

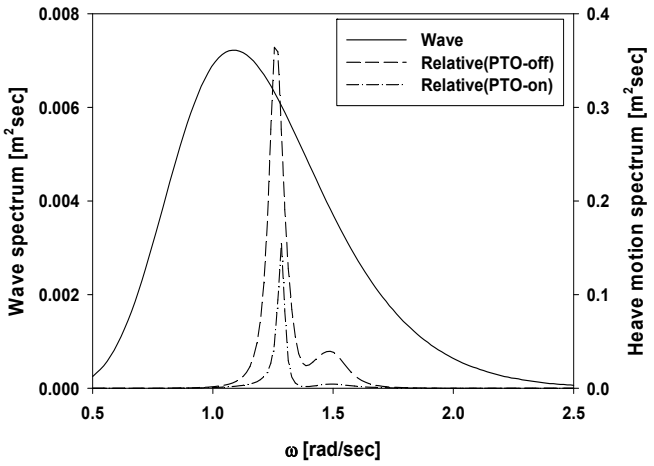

Fig. 8 Relative heave motion spectrum at W1.

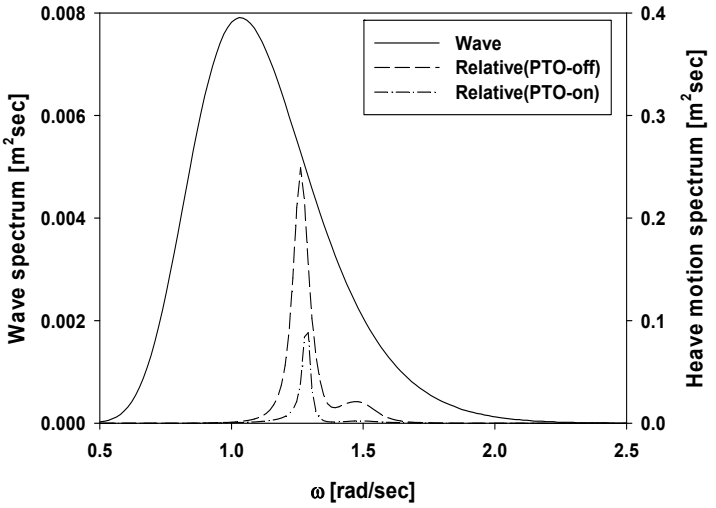

Fig. 9 Relative heave motion spectrum at W2.

Table 4 Significant wave height and heave motion amplitude at W1 and W2.

	W1		W2	
(a) significant wave height based on total wave data ($H_{1/3},[m]$)	0.72		0.94	
(b) significant wave height based on selected wave data ($H_{1/3},[m]$)	0.30		0.27	
	PTO-off	PTO-on	PTO-off	PTO-on
(c) significant relative heave amplitude based on selected wave ($(\xi_{1/2})_{1/3}$)	0.41	0.19	0.33	0.15
(d) $RAO = 2(\xi_{1/2})_{1/3} / H_{1/3}$, (c)/(b)	2.73	1.27	2.44	1.11

Table 4 shows the significant wave height and the relative heave amplitude calculated from the area under the curve for each spectrum as an indication of the amount of energy absorbed by the dual-buoy WEC. The significant wave height based on the total wave spectrum was larger at W2 than at W1 but the significant wave height for the selected wave spectrum (which was obtained only from effective waves capable of generating electricity) was slightly greater at W1. Furthermore, the significant relative heave amplitude, which is the key to the extraction of electrical energy, was greater at W1 than at W2. This means that a greater amount of electrical energy can be obtained at W1. The relative heave RAO can be defined by dividing the relative heave motion height by the significant wave height. The RAO was dependent on the proposed dual-buoy WEC's energy absorption capabilities and demonstrated that the extracted power can be high even with low available wave energy using properly designed WECs suited to the wave conditions at the installation site.

CONCLUSION

A dual-buoy WEC that generates power through the relative heave motion between two buoys is proposed. The WEC consists of two concentric floating circular cylinders (an inner and a hollow outer buoy). Multiple resonances are used in the proposed WEC system not only to enhance the energy extraction efficiency, but also to broaden the frequency range available for energy extraction. Three natural frequencies affect the performance of the WEC: the two heave natural frequencies, one for the inner buoy and another for the outer buoy, and the piston-mode natural frequency of the internal fluid. The dual-buoy WEC was applied at two sites in Hupo Harbor and actual wave data measured at the two installation sites were used to produce the input wave spectrum. The relative heave response of the dual-buoy WEC was estimated for the wave spectrum produced using selected wave data with significant wave height less than 0.5 *m* and average period of 4–6 *sec*. The shape of the dual-buoy WEC was determined by distributing multiple natural frequencies with proper frequency differences around the peak frequency of the input wave spectrum. It was found that the relative heave RAO curve shows a double peak pattern at the two resonant frequencies and a comparatively high RAO value between the two resonant frequencies. The comparison of the RAO at W1 and W2 confirms that even sea sites with lower wave energy density could produce more electrical energy with slight modifications of the buoy's shape. The proposed WEC is suitable for sea sites with low wave energy density and future studies need to focus on the effects of the PTO damping coefficient generated when extracting electrical energy through the LEG (liner electric generator) PTO (power-take-off) system together with various types of mechanical damping.

ACKNOWLEDGEMENT

This work was supported by the New & Renewable Energy Unit of the Korea Institute of Energy Technology Evaluation and Planning (KETEP) grant funded by the Korean Ministry of Knowledge Economy (2010302007 0080).

REFERENCES

Bae, Y.H. and Cho, I.H., 2013. Characteristics of the heaving motion of a hollow circular cylinder. *Journal of Ocean Engineering and Technology*, 27(5), pp.43-50.

Boake, C.B., Whittaker, T.J., Folley, M. and Ellen, H., 2002. Overview and initial operational experience of the LIMPET

wave energy plant. *Proceedings of the 12th International Offshore and Polar Engineering Conference*, Kitakyushu, Japan, 26-31 May 2002, pp.586-594.

Budar, K. and Falnes, J., 1975. A resonant point absorber of ocean-wave power. *Nature*, 256(5517), pp.478-479.

Drew, B., Plummer, A. and Sahinkaya, M.N., 2009. A review of the wave energy converter technology. *Proceedings of the Institution of Mechanical Engineers, Part A: Journal of Power and Energy*, 223(8), pp.887-902.

Falnes, J., 2002. *Ocean waves and oscillating systems: linear interactions including wave-energy extraction*. Cambridge: Cambridge University Press.

Fukuda, K., 1977. Behavior of water in a vertical well with the bottom opening of a ship, and its effects on the ship motion. *Journal of the Society of Naval Architects of Japan*, 141, pp.107-122.

Kweon, H.M., Cho, H. and Jeong, W.M., 2013. Wave analysis and spectrum estimation for the optimal design of the wave energy converter in the Hupo coastal sea. *Korean Society of Ocean Engineers*, 25(3), pp.147-153.

Mavrakos, S.A., 2005. Hydrodynamic coefficients in the heave of two concentric surface-piercing truncated circular cylinders. *Applied Ocean Research*, Elsevier, 26(3), pp.84-97.

Mekhiche, M., Edwards, K. and Bretl, J., 2014. System-level approach to the design, development, testing, and validation of wave energy converters at ocean power technologies. *In ASME 2014 33rd International Conference on Ocean, Offshore and Arctic Engineering*, San Francisco, California, USA, 8-13 June 2014, pp.V09BT09A008-V09BT09A008.

Sinha, A., Kamakar, D. and Soares, C. G., 2014. Numerical modeling of array of heaving point absorbers. *1st International Conference on Renewable Energy Offshore*, Lisbon, Portugal, 24-26 November 2014.

Soares, C.G., Bhattacharjee. J. and Karmakar. D., 2014. Overview and prospects for development of wave and offshore wind energy. *Brodogradnja*, 65(2), pp.91-113.

Weber, J., Mouwen, F., Parish, A. and Robertson, D., 2009. Wavebob: research & development network and tools in the context of systems engineering. *Proceedings of the Eighth European Wave and Tidal Energy Conference*, Uppsala, Sweden, 7-10 September 2009, pp.416-420.

Weinstein, A, Fredrikson, G, Parks, M.J, and Nielsen, K., 2004. AquaBuOY-the offshore wave energy converter numerical modeling and optimization. *Oceans'04. MTTS/IEEE Techno-Ocean'04*, 4, pp.1854-1859.